Pipeline to Build and Test Robust 3D T1 Mapping-Based Heart Models for EP Interventions: Preliminary Results

Mengyuan Li[1,2], Maxime Sermesant[3], Sebastian Ferguson[1], Fumin Guo[1,2], Jen Barry[1], Xiuling Qi[1], Peter Lin[1,2], Matthew Ng[1,2], Graham Wright[1,2], and Mihaela Pop[1,2(✉)]

[1] Sunnybrook Research Institute, Toronto, Canada
mihaela.pop@utoronto.ca
[2] Medical Biophysics, University of Toronto, Toronto, Canada
[3] Inria - Epione Group, Sophia Antipolis, France

Abstract. Computational models are powerful tools in electrophysiology (EP), helping us understand and predict arrhythmia associated with heart attack (i.e., myocardial infarction), a major cause of sudden cardiac death. Our broad aim is to combine novel scar imaging methods with fast computational models to enable accurate predictions of electrical wave propagation, and then to test these models in preclinical frameworks prior to clinical translation. In this work we used n = 3 swine with chronic infarct, which underwent MR followed by conventional x-ray guided electro-anatomical EP mapping. For scar imaging, we employed our T1-mapping MR method based on multi-contrast late enhancement (MCLE) at 1 × 1 mm in-plane resolution and 5 mm slice thickness. Next, we used the MCLE images as input to a fuzzy-logic algorithm and segmented the infarcted area into two zones: infarct core IC (dense fibrosis) and grey-zone, GZ (i.e., arrhythmia substrate). We further built 3D heart models from the stack of segmented 2D MCLE images, integrating tissue zones (healthy, IC and GZ) into detailed tetrahedral heart meshes (~1.5 mm element size). Finally, we investigated the accuracy of model predictions by comparing measured maps of activation times (i.e., depolarization times) with simulated maps obtained by employing a macroscopic formalism and reaction-diffusion equations. We obtained an acceptable small mean absolute error between the simulated and measured depolarization times (~12 ms, in average). Future work will focus on refining MR imaging resolution and use the models to guide ablation procedures.

Keywords: Cardiac MRI · T1-mapping · Modelling · Electrophysiology

1 Introduction

Malignant arrhythmia due to high heart rates (e.g. fast ventricular tachycardia, VT) is an important cause of sudden cardiac death in patients with structural disease such as myocardial infarction [1]. During VT, an aberrant electrical wave anchors around

Y. Coudière et al. (Eds.): FIMH 2019, LNCS 11504, pp. 64–72, 2019.
https://doi.org/10.1007/978-3-030-21949-9_8

electrically inert infarct scars, propagating through viable *isthmuses* of slow conductivity (i.e., channels formed by a mixture of viable myocytes and collagen fibrils). For assessment of electrical function and risk of arrhythmia, these patients undergo an invasive x-ray guided catheter-based electrophysiology (EP) study, during which a map of electrical signals are recorded and used to detect the isthmuses within or at the periphery of infarcted areas, followed by an even more invasive test of arrhythmia inducibility. Once identified, the isthmuses (i.e., VT foci) become targets for VT ablation. Unfortunately, the success rate of ablations is currently lower and VT reoccur in >50% of patients [1]. The ablation failure is often due to inadequate substrate identification in electrical maps which are limited to catheter-based invasive recordings acquired only on the surface of the heart.

Owing to its excellent soft-tissue contrast and lack of radiation, MR imaging has found an increasing role in clinical exams prior to EP interventional studies. Non-invasive MRI is now routinely used to provide structural information regarding infarct location and transmural extent, as well as functional information (i.e., wall motion). Typically, late gadolinium enhancement (LGE) imaging is used for scar imaging [2, 3], where the VT substrate is identified as a *'grey zone'* (GZ) due to its intermediate signal intensity (SI) between scar and healthy tissue [4]. Unfortunately, this method has several drawbacks, particularly missing subtle sub-endocardial GZ. An alternative is to use T1-mapping MR methods, which provide superior contrast and sensitivity in scar/GZ detection compared to LGE images [5].

However, the key limitations due to the surface-derived EP maps and to VT test invasiveness still need to be addressed. To overcome them, *computational modelling* tools can be used [6] in combination with scar information from MR imaging to build 3D heart models coupled with numerical methods. These models can simulate in silico the abnormal propagation of electrical waves and predict VT inducibility. We previously built such 3D heart models from ex vivo diffusion tensor MR images of explanted pig hearts with chronic infarction, and then validated the simulated activation maps and VT test outcome vs. EP measurements recorded by conventional x-ray guided electro-anatomical systems [7]. A next logical step is to develop a similar framework using accurate in vivo MR methods.

In this work we propose a novel pipeline to build preclinical 3D heart models from T1-mapping images and to test them using data obtained from in vivo x-ray guided EP studies from a pig model of chronic infarction. Specifically, here we employ our robust scar/GZ segmentation method which was validated against histology [8], and also correct the motion-induced errors during multi-phase T1 image acquisition. Lastly, we compare measured activation times with those simulated using fast computational models. A simplified diagram illustrating various components of the T1-based pipeline is shown in Fig. 1.

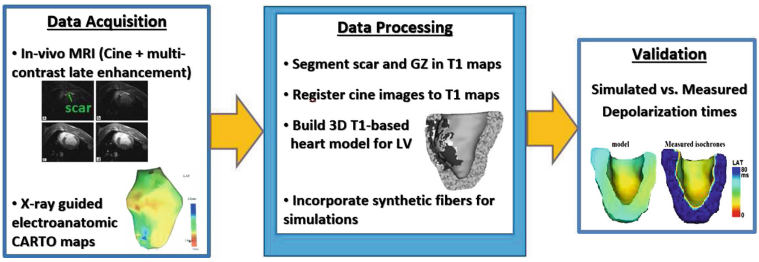

Fig. 1. Diagram for the pipeline to build and test 3D T1-mapping models (including: MR-EP data acquisition, image processing and model validation).

2 Materials and Methods

2.1 Animal Preparation

All in vivo animal studies (i.e., infarct creation, MR imaging and EP procedures) were approved by our Sunnybrook Research Institute. In this work we included results from n = 3 MR-EP studies performed in chronically infarcted pigs. For infarction, a major coronary artery was occluded under x-ray by a balloon catheter for 90 min, followed by reperfusion. The pigs were allowed to heal for ~5 weeks prior to MR-EP studies. By this time point, fibrosis had replaced dead myocytes in the infarct core (IC), whereas a mixture of viable and collagen fibrils was found in the peri-infarct (i.e., GZ), as confirmed by collagen-sensitive histological stains.

2.2 Image Analysis Pipeline

Step (1) Data Acquisition: MR Imaging and EP Studies
All MRI studies were performed using a 1.5T GE SignaExcite MR scanner. For heart anatomy we used a 2D Cine SSFP sequence. For scar imaging we used a T1-mapping method based on a 2D multi-contrast late enhancement (MCLE) method. The MCLE images were acquired over one R-R interval about 20 min following the injection of Gd-based contrast agent, resulting in 20 phases (images) per cardiac cycle at different inversion times (one of them nulling the signal from blood and healthy tissue). Both Cine MR images and MCLE images were acquired at $1 \times 1 \times 5$ mm spatial resolution. For the EP study we used an x-ray guided electro-anatomical CARTO system (Biosense). The LV endocardial maps (~120 points/map) were acquired via a catheter introduced in the LV cavity, in sinus rhythm and/or pacing conditions. In the case of pacing at CL = 500 ms, a second (pacing) catheter was inserted in the RV and positioned at the apex, while the mapping catheter recorded the intracardiac electrograms from the LV-endo. The MR images helped guide the mapping catheter such that denser EP points (~2–3 mm apart) were acquired from within the infarct area.

Step (2) Data Processing: Image Analysis and 3D Heart Model Building
Segmentation: The MCLE images were used to extract steady-state (SS) and T1* maps (Fig. 2a), which were used as an input to a robust fuzzy-logic segmentation algorithm (Matlab). The resulting clusters of healthy, GZ, dense scar (IC) and blood pixels

(Fig. 2b), were used to generate tissue parametric maps (Fig. 2c), which were compared to tissue histological maps using collagen-sensitive stains (Fig. 2d).

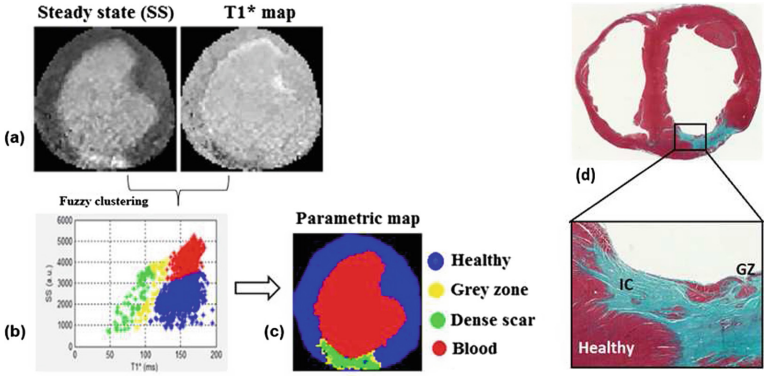

Fig. 2. Segmented MCLE image (a–c). Corresponding histology stain (Masson's Trichrome): IC (dense collagen) in green, GZ as a mixture of green and red, and healthy tissue in dark red (d). (Color figure online)

Image Registration: Prior to building 3D heart models from stacks of 2D segmented MCLE images, we performed a motion correction step to align all segmented MCLE images in the same cardiac phase. To do so, we selected a diastole phase in the Cine sequence, and registered segmented MCLE and Cine images for this phase as in [9]. The MCLE-cine image alignment was initialized using a block-matching-based rigid registration approach [10] followed by a deformable registration refinement step. The deformable registration approach employed [11]: a self similarity context descriptor for image similarity measurements; optical flow as a transformation model; and a convex optimization to derive the optimal solution.

Mesh and Fibers Integration: Our generated 3D MCLE-based LV meshes were constructed using CGAL libraries (www.cgal.org) from the stacks of segmented 2D T1-SS images. These meshes were of sufficiently high density (i.e., between 150–200 K tetrahedral elements, with mean element size 1.3–1.5 mm) to adequately simulate the wave propagation. All 3D heart meshes integrated synthetic fiber directions, which were generated using rule-based methods that obey analytical equations [12].

Step (3) Computational Modelling and Validation Tests

The 3D MCLE-based heart models were further used to simulate the electrical wave propagation through the heart using a mono-domain macroscopic formalism with reaction-diffusion equations. This model proposed by Aliev-Panfilov model [13, 14] solves for the action potential (V) and recovery term (r), and was implemented by Inria researchers [15]:

$$\frac{\partial V}{\partial t} = \nabla \cdot (D\nabla V) - kV(V-a)(V-1) - rV \tag{1}$$

$$\frac{\partial r}{\partial t} = -(\varepsilon + \frac{\mu_1 r}{\mu_2 + V})(kV(V-a-1)+r) \tag{2}$$

where a tunes the action potential duration and k corresponds to the recovery phase. This fiber directions are accounted for via the diffusion tensor D, where d is the 'bulk' electrical conductivity of tissue. A reduced value of d results in a low conduction velocity (c) of wave:

$$c = \sqrt{2 \cdot k \cdot d}(0.5 - a) \tag{3}$$

In this work we personalized only the key model parameter 'd' corresponding to the tissue electrical conductivity, because we compared only the simulated and measured maps of depolarization times, whereas the other parameters were taken from previous studies [7, 15]. We calibrated *d_healthy* in the healthy zone by employing a calibration curve [16]. We then assigned *d_GZ* = 0.5**d_healthy* to the slow-conductive GZ, and *d_scar* = 0 to the non-conductive scar, as in [7, 17].

For all Finite Element simulations, we used a 4,096(1x)MB machine with an Intel® Core™ i3-2310M processor, 640 GB HD, NVIDIA® GeForce® 315M graphic adapter. Typically, it took <5 min to simulate 200 ms of the cardiac cycle on a mesh of about 150K elements (~1.5 mm element size).

Lastly, we compared the simulated and measured depolarization time maps. For quantitative comparisons, we projected the point-based measured endocardial maps onto the LV surfaces of each mesh, and then we interpolated these maps using our image visualization platform, Vurtigo (www.vurtigo.ca).

3 Results

Figure 3 shows results from the MCLE-to-Cine MR image registration step, before (*left*) and after (*right*) motion correction of the myocardial wall seen in a longitudinal view through the heart segmented in Fig. 2. The registration process was automated, requiring approximatively 3 min per heart. Note the improved alignment of the myocardial contours with Dice coefficients (%) of ~82%, which resulted in smooth endocardial/epicardial surfaces of the 3D LV model.

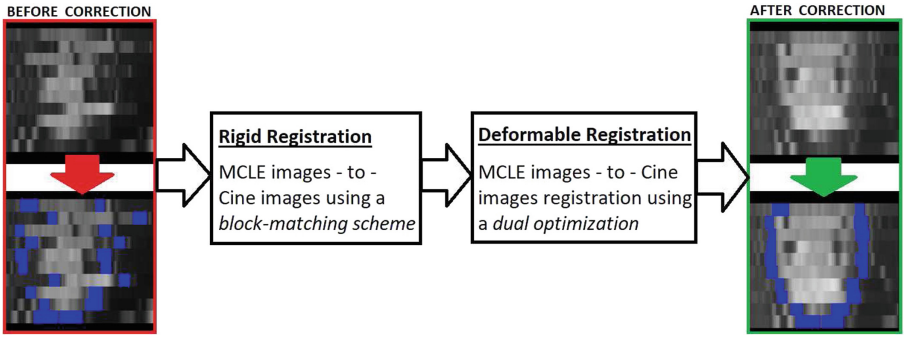

Fig. 3. Motion correction performed through the MCLE-to-Cine image registration, resulting in smoothly aligned endocardial/epicardial surfaces

Next, exemplary results from the construction of a 3D LV model for one infarcted pig heart are presented in Fig. 4. From the stack of 2D segmented MCLE images (registered to the Cine images as described above), we generated an interpolated 3D anatomical LV model using CGAL libraries. The model integrated the three classes of tissue (i.e., healthy zone, GZ and infarct core, IC) determined from the T1-SS mapping images (Fig. 4a). In addition, shown are also the tetrahedral mesh (Fig. 4b) as well as synthetic fibers rotating from −70° to +70° (from endocardium to epicardium) integrated into the 3D LV mesh by assigning the fiber directions to each vertex (Fig. 4c).

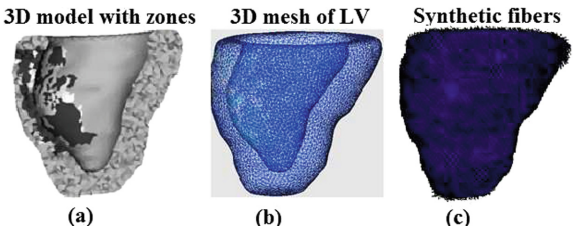

Fig. 4. Results from building a T1-based model for an infarcted pig heart: (a) 3D LV anatomic model integrating the three MCLE-defined tissue zones (GZ area is in white and the IC area is in black); (b) corresponding mesh (∼150K elements); and (c) synthetic fibers.

Figure 5 shows LV models integrating various fiber inclinations. Based on our previous work [7, 17] and comparisons with EP data in healthy hearts, our results suggest that an angle inclination range of [−70°/+70°] produces the closest pattern and smallest error between simulated and measured endocardial activation maps.

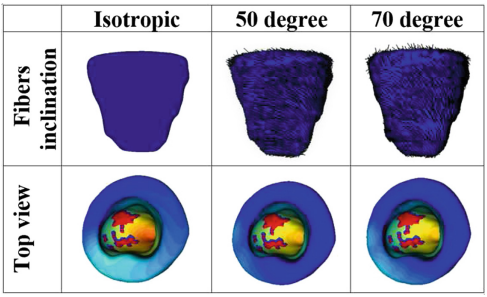

Fig. 5. Simulated activation times for LV modes with different fibers inclinations

Figure 6a shows the calibration curve for the speed of wave vs. *d_healthy* (bulk conductivity) used for model personalization. Figure 6b shows simulated depolarization times (left) and experimental maps (*right*), with LAT being the local activation time (*blue* corresponds to late depolarization times). The scar (IC) was assigned $d = 0$. The simulations on this LV mesh were performed in ∼4 min.

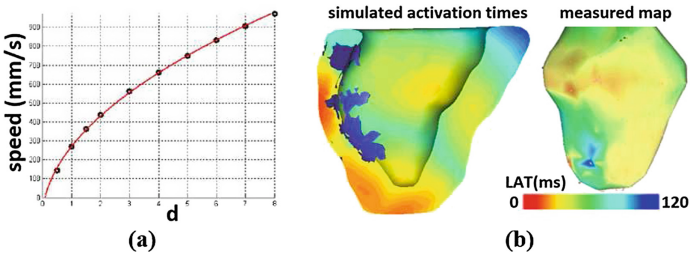

Fig. 6. Results: calibration curve for speed vs *d* conductivity (a); and comparison between the simulated and measured depolarization maps in an infarcted heart (b).

Overall, there was a very good qualitative correspondence between computed and measured activation patterns in all three infarcted hearts. Furthermore, quantitative comparison led to an acceptable absolute error ($\sim$12 ms mean values, in average among the three hearts) between the simulated depolarization times vs. measured depolarization maps recorded from the endocardial surface. The largest differences were observed at the periphery of infarct, which was expected due to the relatively sparse EP points compared to the MR-derived mesh density. All quantitative comparisons were performed using custom codes developed in Matlab.

4 Discussion and Future Work

Innovative biomedical technologies using exquisite cardiac MR scar imaging methods in combination with predictive image-based computer models can used as powerful non-invasive diagnostic and treatment-planning tools in the clinical EP lab. To sum up, in this work we proposed a novel image analysis pipeline to augment the information from conventional electro-anatomical EP studies with 3D electro-physiology simulations using high-resolution T1-mapping-based computer models. Such models could supplement important information that is currently lacking in EP maps due to the sparse point-base recordings, typically limited to the LV endocardial surface. Our T1-mapping MCLE method for scar imaging was recently validated using quantitative histopathology [8], giving us confidence that our 3D anatomical models integrating three zones: scar, healthy tissue and GZ are sufficiently accurate.

The preclinical results in this work suggest that macroscopic theoretical models can provide rapid (<5 min) simulation results for depolarization times on relatively dense MCLE-derived LV meshes, making them attractive for rapid integration into clinical platforms. Although these preliminary results are promising, we acknowledge that a modelling limitation was the usage of *global* parameters (i.e., same conductivity or speed within the healthy LV tissue). Better predictions may be obtained if the key parameters in the model will be calibrated locally, using AHA-based 17 segments for LV [18]. Thus, future work will focus on personalizing *local* model parameters per individual heart from EP data using these AHA segments. We envision that this refined approach will improve the model personalization and further reduce the error between

simulated and measured activation times. We also aim to include the right ventricle into 3D biventricular heart meshes and simulate the VT inducibility.

Lastly, for rapid scar/GZ imaging we are currently developing and testing a high-resolution 3D MCLE method with navigator, which produces an excellent contrast at blood-tissue interface at a 1.5 mm isotropic spatial resolution [19]. This voxel size can overcome potential partial volume effects in the scar/GZ segmentation obtained at the $1 \times 1 \times 5$ mm resolution. This 3D MCLE method will also help avoiding any potential errors introduced by cardiac and respiratory motion in the segmentation/registration steps. Thus, we anticipate that 3D heart models built from high resolution MCLE images will provide robust identification of the VT substrate and a better guidance of the RF ablation procedure.

5 Conclusion

Our broad goal is to test the predictive power of our 3D T1-based models and predict risk of scar-induced arrhythmias. Here, we proposed a pipeline to build and test predictive T1-mapping image-based computer models using a preclinical pig model of infarction that mimics very well the human pathophysiology of chronic scars. Overall, our novel 3D computer LV models can give superior information compared to the surface EP maps, allowing for visualization of transmural activation times and activation patterns through the myocardial wall, relative to the precise position of the scar in the infarcted hearts.

Acknowledgement. The authors acknowledge funding from CIHR grants (Dr. Pop and Dr. Wright) and Inria *Associate project* (Dr. Sermesant and Dr. Pop). Megyuan Li was supported in part by a summer student UROP – Medical Biophysics award.

References

1. Stevenson, W.G.: Ventricular scars and VT tachycardia. Trans. Am. Clin. Assoc. **120**, 403–412 (2009)
2. Bello, D., Fieno, D.S., Kim, R.J., et al.: Infarct morphology identifies patients with substrate for sustained ventricular tachycardia. J. Am. Coll. Cardiol. **45**(7), 1104–1110 (2005)
3. Codreanu, A., Odille, F., et al.: Electro-anatomic characterization of post-infarct scars comparison with 3D myocardial scar reconstruction based on MRI. J. Am. Coll. Cardiol. **52**, 839–842 (2008)
4. Wijnmaalen, A., et al.: Head-to-head comparison of c-e MRI and electroanatomical voltage mapping to assess post-infarct scar characteristics in patients with VT: real-time image integration and reversed registration. Eur. Heart J. **32**, 104 (2011)
5. Detsky, J.S., Paul, G., Dick, A.J., Wright, G.A.: Reproducible classification of infarct heterogeneity using fuzzy clustering on multi-contrast delayed enhancement MR images. IEEE Trans. Med. Imaging **28**(10), 1606–1614 (2009)
6. Clayton, R.H., Panfilov, A.V.: A guide to modelling cardiac electrical activity in anatomically detailed ventricles. Prog. Biophys. Mol. Biol. Rev. **96**(1–3), 19–43 (2008)

7. Pop, M., et al.: Correspondence between simple 3D MR image-based heart models and in-vivo EP measures in swine with chronic infarction. IEEE Trans. Biomed. Eng. **58**(12), 483–3486 (2011)
8. Pop, M., Ramanan, V., Yang, F., Zhang, L., Newbigging, S., Wright, G.: High resolution 3D T1* mapping and quantitative image analysis of the 'gray zone' in chronic fibrosis. IEEE Trans. Biomed. Eng. **61**(12), 2930–2938 (2014)
9. Guo, F., Li, M., Ng, M., Wright, G., Pop, M.: Cine and multicontrast late enhanced MRI registration for 3D heart model construction. In: Pop, M., et al. (eds.) STACOM 2018. LNCS, vol. 11395, pp. 49–57. Springer, Cham (2019). https://doi.org/10.1007/978-3-030-12029-0_6
10. Ourselin, S., Roche, A., Prima, S., Ayache, N.: Block matching: a general framework to improve robustness of rigid registration of medical images. In: Delp, Scott L., DiGoia, Anthony M., Jaramaz, B. (eds.) MICCAI 2000. LNCS, vol. 1935, pp. 557–566. Springer, Heidelberg (2000). https://doi.org/10.1007/978-3-540-40899-4_57
11. Heinrich, M.P., Jenkinson, M., Papież, B.W., Brady, S.M., Schnabel, J.A.: Towards realtime multimodal fusion for image-guided interventions using self-similarities. In: Mori, K., Sakuma, I., Sato, Y., Barillot, C., Navab, N. (eds.) MICCAI 2013. LNCS, vol. 8149, pp. 187–194. Springer, Heidelberg (2013). https://doi.org/10.1007/978-3-642-40811-3_24
12. Arts, T., Costa, K.D., Covell, J.W., McCulloch, A.D.: Relating myocardial laminar architecture to shear strain and muscle fiber orientation. Am. J. Physiol. Heart Circ. Physiol. **280**(5), H2222–2229 (2001)
13. Aliev, R., Panfilov, A.V.: A simple two variables model of cardiac excitation. Chaos Soliton Fractals **7**(3), 293–301 (1996)
14. Nash, M.P., Panfilov, A.V.: Electromechanical model of excitable tissue to study reentrant cardiac arrhythmias. Prog. Biophys. Mol. Biol. **85**, 501–522 (2004)
15. Sermesant, M., Delingette, H., Ayache, N.: An electromechanical model of the heart for image analysis and simulation. IEEE Trans. Med. Imaging **25**(5), 612–625 (2006)
16. Chinchapatnam, P., Rhode, K.S., Ginks, M., et al.: Model-based imaging of cardiac apparent conductivity and local conduction velocity for planning of therapy. IEEE Trans. Med. Imaging **27**(11), 1631–1642 (2008)
17. Pop, M., Sermesant, M., Liu, G., Relan, J., et al.: Construction of 3D MR image-based computer models of pathologic hearts, augmented with histology and optical imaging to characterize the action potential propagation. Med. Image Anal. **16**(2), 505–523 (2012)
18. Cerqueira, M.D., Weissman, N.J., et al.: Standardized myocardial segmentation and nomenclature for tomographic imaging of the heart: a statement for health-care professionals from the Cardiac Imaging Committee of the Council on Clinical Cardiology of the American Heart Association. Circulation **105**, 539–542 (2002)
19. Zhang, L., Athavale, P., Pop, M., Wright, G.: Multi-contrast reconstruction using compressed sensing with low rank and spatially-varying edge-preserving constraints for high-resolution MR characterization of infarction. Magn. Reson. Med. **78**, 598–610 (2016)